Check for updates

Received: 15 October 2024 | Revised: 13 January 2025 | Accepted: 14 January 2025

DOI: 10.1002/alz.14600

Alzheimer's & Dementia®
THE JOURNAL OF THE ALZHEIMER'S ASSOCIATION

RESEARCH ARTICLE

# Machine learning prediction of tau-PET in Alzheimer's disease using plasma, MRI, and clinical data

**Linda Karlsson**[1] | **Jacob Vogel**[2] | **Ida Arvidsson**[3] | **Kalle Åström**[3] | **Olof Strandberg**[1] | **Jakob Seidlitz**[4,5,6,7] | **Richard A. I. Bethlehem**[8] | **Erik Stomrud**[1,9] | **Rik Ossenkoppele**[1,10] | **Nicholas J. Ashton**[11,12] | **Henrik Zetterberg**[11,13,14,15,16,17] | **Kaj Blennow**[11,13,18,19] | **Sebastian Palmqvist**[1,9] | **Ruben Smith**[1,9] | **Shorena Janelidze**[1] | **Renaud La Joie**[20] | **Gil D. Rabinovici**[20,21] | **Alexa Pichet Binette**[1] | **Niklas Mattsson-Carlgren**[1,9] | **Oskar Hansson**[1]

[1]Clinical Memory Research Unit, Department of Clinical Sciences Malmö, Lund University, Lund, Sweden

[2]Department of Clinical Sciences, SciLifeLab, Lund University, Lund, Sweden

[3]Centre for Mathematical Sciences, Lund University, Lund, Sweden

[4]Penn/CHOP Lifespan Brain Institute, University of Pennsylvania, Philadelphia, Pennsylvania, USA

[5]Department of Psychiatry, University of Pennsylvania, Philadelphia, Pennsylvania, USA

[6]Department of Child and Adolescent Psychiatry and Behavioral Science, The Children's Hospital of Philadelphia, Philadelphia, Pennsylvania, USA

[7]Institute for Translational Medicine and Therapeutics, University of Pennsylvania, Philadelphia, Pennsylvania, USA

[8]University of Cambridge, Department of Psychology, Cambridge Biomedical Campus, Cambridge, UK

[9]Memory Clinic, Skåne University Hospital, Malmö, Sweden

[10]Alzheimer Center Amsterdam, Department of Neurology, Amsterdam Neuroscience, Amsterdam UMC, Amsterdam, the Netherlands

[11]Department of Psychiatry and Neurochemistry, Institute of Neuroscience and Physiology, the Sahlgrenska Academy, University of Gothenburg, Mölndal, Sweden

[12]Institute of Psychiatry, Psychology and Neuroscience, Maurice Wohl Institute Clinical Neuroscience, King's College London, London, UK

[13]Clinical Neurochemistry Laboratory, Sahlgrenska University Hospital, Mölndal, Sweden

[14]Department of Neurodegenerative Disease, UCL Institute of Neurology, Queen Square, London, UK

[15]UK Dementia Research Institute at UCL, London, UK

[16]Hong Kong Center for Neurodegenerative Diseases, 5/F, Building 5E, 5 Science Park East Avenue, Hong Kong Science Park, Clear Water Bay, Hong Kong, China

[17]Wisconsin Alzheimer's Disease Research Center, University of Wisconsin School of Medicine and Public Health, University of Wisconsin-Madison, Madison, Wisconsin, USA

[18]Paris Brain Institute, ICM, Pitié-Salpêtrière Hospital, Sorbonne University, Paris, France

[19]Neurodegenerative Disorder Research Center, Division of Life Sciences and Medicine, and Department of Neurology, Institute on Aging and Brain Disorders, University of Science and Technology of China and First Affiliated Hospital of USTC, Hefei, Anhui, P.R. China

[20]Department of Neurology, Memory and Aging Center, Weill Institute for Neurosciences, University of California, San Francisco, California, USA

[21]Department of Radiology and Biomedical Imaging, University of California, San Francisco, San Francisco, California, USA

**Correspondence**
Linda Karlsson and Oskar Hansson, Clinical Memory Research Unit, Department of Clinical Sciences Malmö, BMC C11, Lund University, Box 117, SE-22100 Lund, Sweden.
Email: linda.karlsson@med.lu.se and oskar.hansson@med.lu.se

## Abstract

**INTRODUCTION:** Tau positron emission tomography (PET) is a reliable neuroimaging technique for assessing regional load of tau pathology in the brain, but its routine clinical use is limited by cost and accessibility barriers.

This is an open access article under the terms of the Creative Commons Attribution-NonCommercial License, which permits use, distribution and reproduction in any medium, provided the original work is properly cited and is not used for commercial purposes.
© 2025 The Author(s). *Alzheimer's & Dementia* published by Wiley Periodicals LLC on behalf of Alzheimer's Association.

**Funding information**
Science for Life Laboratory, Grant/Award Number: KAW 2020.0239; Skånes universitetssjukhus, Grant/Award Number: 2020-O000028; EU Joint Programme – Neurodegenerative Disease Research, Grant/Award Number: 2019-03401; Parkinsonfonden, Grant/Award Number: 1412/22; Hjärnfonden, Grant/Award Numbers: FO2021-0293, FO2023-0163; Alzheimerfonden, Grant/Award Numbers: AF-980907, AF-994229; Knut och Alice Wallenbergs Stiftelse, Grant/Award Number: 2022-0231; Vetenskapsrådet, Grant/Award Numbers: 2022-00775, 2021-02219, 2018-02052; Alzheimer's Association, Grant/Award Numbers: ZEN24-1069572, SG-23-1061717; H2020 European Research Council, Grant/Award Number: ADG-101096455; National Institute on Aging, Grant/Award Number: R01AG083740; WASP and DDLS Joint call for research projects, Grant/Award Number: WASP/DDLS22-066

**METHODS:** We thoroughly investigated the ability of various machine learning models to predict clinically useful tau-PET composites (load and laterality index) from low-cost and non-invasive features, for example, clinical variables, plasma biomarkers, and structural magnetic resonance imaging (MRI).

**RESULTS:** Models including plasma biomarkers yielded the most accurate predictions of tau-PET burden (best model: *R*-squared = 0.66–0.69), with especially high contribution from plasma phosphorylated tau-217 (p-tau217). MRI variables were the best predictors of asymmetric tau load between the two hemispheres (best model: *R*-squared = 0.28–0.42). The models showed high generalizability to external test cohorts with data collected at multiple sites. Through a proof-of-concept two-step classification workflow, we also demonstrated possible model translations to a clinical setting.

**DISCUSSION:** This study highlights the promising and limiting aspects of using machine learning to predict tau-PET from scalable cost-effective variables, with findings relevant for clinical settings and future research.

**Highlights**

- Accessible variables showed potential in estimating tau tangle load and distribution.
- Plasma phosphorylated tau-217 (p-tau217) and magnetic resonance imaging (MRI) were the best predictors of different tau-PET (positron emission tomography) composites.
- Machine learning models demonstrated high generalizability across AD cohorts.

## 1 | INTRODUCTION

Alzheimer's disease (AD) is the most common neurodegenerative disease, with prevalence continuing to increase worldwide.[1] It is characterized by pathological aggregation of amyloid beta (A$\beta$) plaques and neurofibrillary tau tangles in the brain. AD pathology can be reliably detected and quantified using fluid or imaging biomarkers, for example, plasma (blood-based), cerebrospinal fluid (CSF), or positron emission tomography (PET).[2,3] These AD biomarkers vary in availability, cost, invasiveness, and comprehensiveness, and the most demanding methods are not feasible to implement in larger populations, even if they may be the most reliable and informative ones. Amyloid- and tau-PET are the only methods to spatially resolve AD pathology in the living human brain, but they are expensive and not readily available in most clinical settings.[4] Conversely, plasma biomarkers are or will likely be highly accessible and minimally invasive, and although capturing a variety of biological aspects related to AD, they lack detail on spatial resolution of the pathology. Structural magnetic resonance imaging (MRI) represents a relatively lower-cost alternative to spatially measure in vivo neurodegeneration, but it is substantially less specific to AD pathology compared to PET.[5–8] With emerging disease-modifying therapies for AD,[9,10] including tau-targeting therapies under development,[11] it is crucial to find ways to reduce the need for PET scans due to their relative inaccessibility and costliness, while still preserving the ability to estimate the load and distribution of AD pathology as accurately and comprehensively.[12,13]

In this work, we specifically aim to address the problem of limited global access to tau-PET. Tau-PET is often considered a state-of-the-art outcome in AD research studies, a very accurate prognostic tool in patients with AD, and frequently used in clinical trials for AD during screening and to monitor treatment effects.[12,14–16] Furthermore, tau-PET provides information beyond what can be captured by other imaging modalities or fluid biomarkers, including in vivo assessment of Braak stages, which indicates the progression of tau pathology throughout the brain.[17,18] Even though tau pathology often spreads in a distinct spatial pattern, recent work has provided insights into the heterogeneity of the disease by characterizing different subtypes of the tau deposition patterns, which can be of relevance for an individually adapted prognosis.[19,20] Asymmetry in tau accumulation between the two hemispheres can, for example, offer clues about the lateralization of pathology within the brain.[21–23] Such asymmetry can give rise to atypical clinical profiles, related to, for example, behavioral and cognitive differences,[24] and has been shown to relate to faster disease progression.[19]

Here, we thoroughly investigate the ability of machine learning (ML) models to predict tau-PET composites from a broad range of low-cost and non- or minimally invasive variables only. We aim to understand the scope of available features as tools predictive of tau pathology

15525279, 2025, 2, Downloaded from https://alz-journals.onlinelibrary.wiley.com/doi/10.1002/alz.14400, Wiley Online Library on [11/08/2025]. See the Terms and Conditions (https://onlinelibrary.wiley.com/terms-and-conditions) on Wiley Online Library for rules of use; OA articles are governed by the applicable Creative Commons License

(load and distribution), and to explore the potential of their expanded utility in a context where invasive and/or expensive procedures are not available. Specifically, we investigated how well two different tau-PET composites can be predicted from basic clinical variables, plasma AD biomarkers, and structural MRI-derived morphology. These two composites were: (1) tau load in the temporal cortex (an early, sensitive, and commonly used composite marker of tau deposition in AD) and (2) hemispheric asymmetry of temporal lobe tau load in tau positive participants (as an example of clinically relevant spatial tau PET information). Toward this purpose, we created a flexible and ambitious ML pipeline, evaluating various ML estimators, and designed to handle both different feature types and different number of input features for classification and regression tasks. We evaluated the results on an unseen test set and multiple external cohorts. We further investigated feature contribution for increased model interpretability and transparency. Finally, we created a two-step pipeline proposed to simulate how the findings could be implemented in a clinical setting without access to tau-PET.

**RESEARCH IN CONTEXT**

1. **Systematic review**: We reviewed the literature using traditional sources. The relationships of the accessible variables with tau-PET (positron emission tomography) have been heavily researched, but usually in inferential settings rather than predictive, mainly looking at linear associations instead of more complex relationships within the data using machine learning, for smaller samples sizes, and rarely incorporating multiple levels of data in the same model.
2. **Interpretation**: Our findings highlight both the promising and limiting aspects of using machine learning to predict tau-PET composites. Key variables align with findings in the previous literature.
3. **Future directions**: The work enhances understanding of combining cost-effective variables from multiple modalities for tau-PET prediction. The results have implications for future research aimed at synthesizing full tau-PET scans. The two-step model for clinical use needs improvement but has the potential of being useful in contexts where tau-PET is not available. For further improvement, we recommend training on larger samples, more specific biomarkers (e.g., microtubule-binding region of tau MTBR-tau243), and more diverse populations.

## 2 | MATERIALS AND METHODS

### 2.1 | Participants

Participants who had undergone thorough expert clinical assessments, tau-PET, MRI, and plasma collection were included from two study cohorts: the Swedish BioFINDER-2 (BF2) cohort (enrollment between 2017 and 2022, $n = 1195$, NCT03174938) and the Swedish BioFINDER-1 (BF1) cohort (enrollment between 2010 and 2015, $n = 147$, NCT01208675). The participants were individuals with normal cognition (NC, $n = 321$ in BF2 and $n = 54$ in BF1), subjective cognitive decline (SCD, $n = 153$ in BF2 and $n = 9$ in BF1), mild cognitive impairment (MCI, $n = 236$ in BF2 and $n = 25$ in BF1), dementia ($n = 232$, of which 136 were AD and 96 non-AD cases in BF2 and $n = 41$, of which 34 were AD and 7 non-AD cases in BF1), or another neurodegenerative disease ($n = 6$ in BF2 and $n = 18$ in BF1). All participants in BF2 and BF1 were recruited at Skåne University Hospital or the Hospital of Ängelholm, Sweden. AD dementia was diagnosed according to the Diagnostic and Statistical Manual of Mental Disorders, Fifth Edition (DSM-5) AD criteria and A$\beta$ positivity. Further details about BF2 and BF1 have been described in previous works.[25,26] Detailed demographics are presented in Table S1.

Participants who had undergone clinical assessments, tau-PET, and MRI were included from four additional study cohorts: the Alzheimer's Disease Neuroimaging Initiative cohort (ADNI; http://adni.loni.usc.edu; $n = 213$), University of California San Francisco Alzheimer's Disease Research Center cohort (UCSF-ADRC; $n = 196$),[27,28] the Anti-Amyloid Treatment in Asymptomatic AD cohort (A4; $n = 45$),[29,30] and Open Access Series of Imaging Studies phase 3 (OASIS-3; $n = 46$).[31] ADNI is a publicly available cohort, aimed for use in research studies investigating AD progression. Participants were recruited across centers in North America. The UCSF-ADRC maintains a research clinical cohort, including participants with different neurodegenerative diseases and at various stages of cognitive decline. A4 is a secondary prevention trial in preclinical AD, including cognitively unimpaired A$\beta$-positive participants (based on A$\beta$-PET). The data used in this work were collected before randomization to treatment arms. OASIS3 is a publicly available cohort study generated by the Knight ADRC and its affiliated studies, including participants at various stages of cognitive decline. Demographics on all cohorts are presented in Table S1.

### 2.2 | Ethics

All protocols were approved by each cohort's respective institutional ethical review board, and all participants gave written informed consent.

### 2.3 | Plasma collection and analysis

BF2 and BF1 plasma samples were collected at baseline and handled according to established preanalytical protocols, previously described in detail for both cohorts.[25,32] All analyses were performed by technicians blinded to all clinical and imaging data. Plasma biomarkers were measured with Eli Lilly assays on a Meso Scale Discovery platform (phosphorylated tau-217 [p-tau217] and p-tau181)[25] or with

15525279, 2025, 2, Downloaded from https://alz-journals.onlinelibrary.wiley.com/doi/10.1002/alz.14600, Wiley Online Library on [11/08/2025]. See the Terms and Conditions (https://onlinelibrary.wiley.com/terms-and-conditions) on Wiley Online Library for rules of use; OA articles are governed by the applicable Creative Commons License

Simoa immunoassays developed at the University of Gothenburg (p-tau231, N-terminal containing tau fragments [NTA], glial fibrillary acidic protein [GFAP], and neurofilament light [NfL]).[33–35] In UCSF-ADRC, plasma p-tau217 was measured with Eli Lilly assays on a Meso Scale Discovery platform.[36] In ADNI, plasma biomarkers were measured with Fujirebio Lumipulse assay (p-tau217) and Roche NeuroToolKit assays (p-tau181, GFAP, and NfL).[37] We bridged the plasma p-tau217 Fujirebio Lumipulse and Lilly assays using $n = 1374$ in-house samples.

## 2.4 | Tau-PET and MR imaging

In BF2, tau-PET was performed using [$^{18}$F]RO948. Standardized uptake value ratio (SUVR) images were created for the 70–90 min post-injection interval using the inferior cerebellar cortex as reference region. In BF1, ADNI, UCSF-ADRC, OASIS3, and A4, tau-PET was performed using [$^{18}$F]flortaucipir. SUVR images were created for the 80–100 post-injection interval using the inferior cerebellar cortex as reference region. T1-weighted volumetric MRI scans were segmented using FreeSurfer v.6.0 (https://surfer.nmr.mgh.harvard.edu/), resulting in native space parcellations of each participant's brain using the Desikan–Killiany (FreeSurfer) atlas. The parcellations were also used to extract mean SUVR values in regions of interest (ROIs) for each participant in native space. All MRI and tau-PET images were processed locally at Lund University, following the same pipeline described previously across studies.[38]

## 2.5 | Tau-PET prediction outcomes

Two tau-PET indices were predicted in this work: tau-PET Braak I-IV load, corresponding to a temporal meta-ROI, and tau-PET Braak I-IV laterality index (LI).

### 2.5.1 | Braak I-IV load

The first tau-PET outcome we defined as a continuous load composite variable, corresponding to Braak I-IV regions (entorhinal, amygdala, parahippocampal, fusiform, and inferior and middle temporal ROIs[17]). The composite was dichotomized according to previously established cutoffs: positivity > 1.36 for [$^{18}$F]RO948 and > 1.34 for [$^{18}$F]flortaucipir.[6,39] See Figure 1A and 1B for the distribution of this outcome variable in all cohorts plotted against LI, and Figure 1C for examples of tau-PET scans with low and high load. Corresponding scatter plots against age are provided in Figure S1.

### 2.5.2 | Laterality index

The second tau-PET outcome we defined as asymmetry in the temporal meta-ROI computed as a LI. The index was formulated as the difference between the left and right hemispheres normalized to the average signal in the left and right hemispheres, as was done in, for example,[40,41]

$$\text{laterality index} = \frac{100}{N}\sum_{i=1}^{N}\frac{x_{i,Left} - x_{i,Right}}{\left(x_{i,Left} + x_{i,Right}\right)/2}, \quad (1)$$

where $x_i$ is the SUVR of brain region $i$ and $N$ is the total number of brain regions used. To make the LI specific for the Braak I-IV composite, only brain regions in Braak I-IV were used for $i$, $x_i$, and $N$. A negative LI represents more tau in the right hemisphere than the left and vice versa. Because the index was normalized to the total amount of tau load in the Braak I-IV composite, a more clinically relevant and dispersed distribution was achieved when including only individuals categorized as tau-positive (Figure 1A, B). See Figure 1C for examples of symmetric and asymmetric tau-PET scans in this ROI. For classification tasks, a lower and upper threshold of the composite was computed in the BF2 training cohort as the mean value plus/minus two standard deviations in the tau-negative group: −7.61 and 7.27. Tau-positive participants were divided into three corresponding classes: right-asymmetric (LI < −7.61), left-asymmetric (LI > 7.27), or symmetric (−7.61 < LI < 7.27).

## 2.6 | Machine learning pipeline

To search for high-performing hyperparameter-tuned ML estimators, we implemented a flexible and comprehensive ML pipeline, evaluating various ML estimators and designed to handle both different feature types and different number of input features for classification and regression tasks. The pipeline is visualized in Figure 2 and included the following steps:

1. **Standardization**. Performed to get comparable feature scales and numeric adaptation to the estimator's optimization methods.
2. **Feature selection**. Evaluating one of eight different feature selection methods with the aim to, in a data-driven manner, find features with relevant predictive information and remove redundant ones, thereby improving chances of generalizability. The eight methods included variations on percentile-based feature selection, recursive feature elimination, and random forest (RF) selection, and are described in Table S2.
3. **Estimator**. Evaluating one of seven different estimators with the aim of finding the one(s) most suitable for the specific task. The seven methods are described in Table S2, and include linear models, boosted tree-based methods, and support vector machines.
4. **Hyperparameter tuning**. Searching for appropriate hyperparameters through Bayesian optimization. Bayesian optimization is a technique that efficiently explores the hyperparameter space based on past evaluations. It combines probabilistic models, such as Gaussian processes, with an acquisition function to balance exploration and exploitation, ultimately guiding the search toward promising regions of the hyperparameter space.[42,43]

15525279, 2025, 2, Downloaded from https://alz-journals.onlinelibrary.wiley.com/doi/10.1002/alz.14400, Wiley Online Library on [11/08/2025]. See the Terms and Conditions (https://onlinelibrary.wiley.com/terms-and-conditions) on Wiley Online Library for rules of use; OA articles are governed by the applicable Creative Commons License

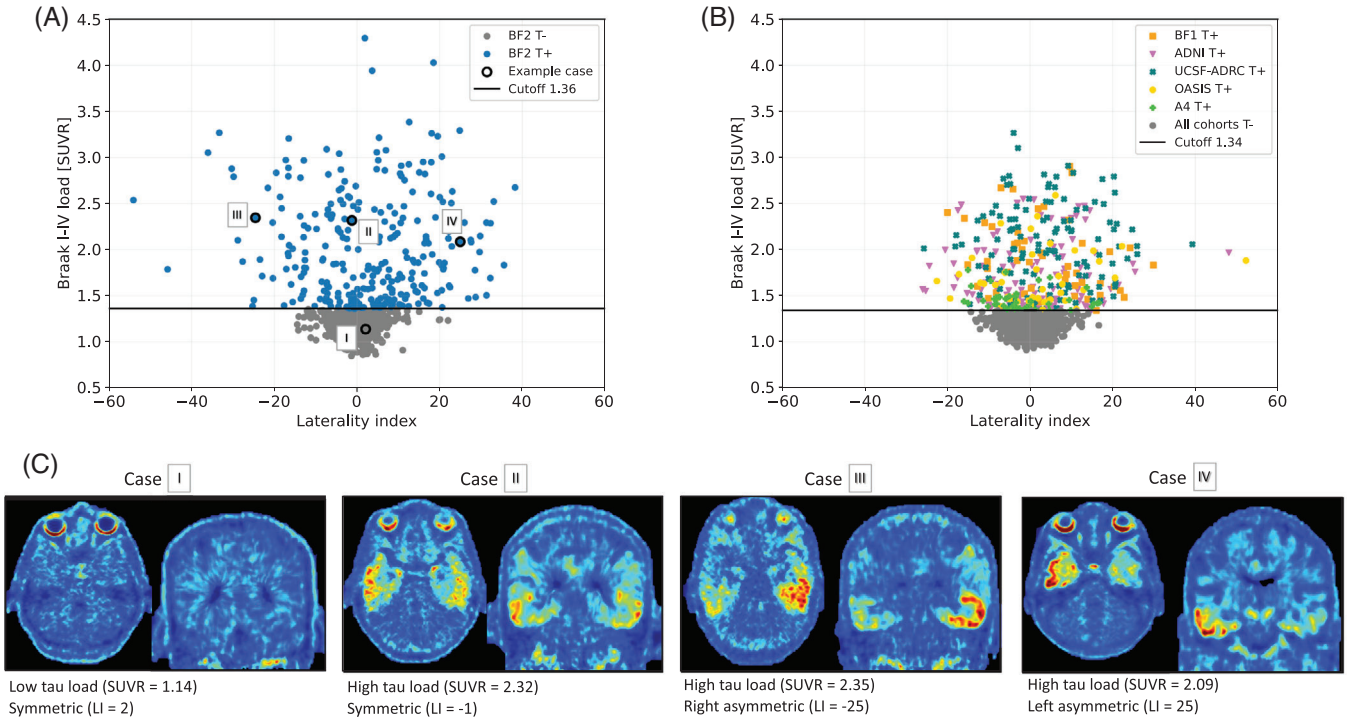


**FIGURE 1** Distribution of the two outcome variables tau-PET Braak I-IV load and laterality index (L > R) in (A) BF2 and (B) external test sets. Note that different tau-PET tracers were used in the cohorts ([$^{18}$F]RO948 in BF2 and [18F]flortaucipir in the others), resulting in slightly different cutoffs for positivity (1.36 and 1.34). (C) tau-PET example cases of low/high tau load, and symmetric/asymmetric tau distribution from BF2 (correspondingly marked out in A). LI, laterality index; SUVR, standardized uptake value ratio.

5. **Evaluation**. Evaluating results on a selected metric relevant to the task at hand. In this work, mean squared error (MSE) was used for all regression tasks and accuracy for all classification tasks.

The full pipeline was optimized in a 10-fold cross-validation setting on training data, where all steps were fitted to the training folds and evaluated only for the validation fold. Steps 2 and 3 were conducted in a grid-search setting to compare all 56 combinations of feature selection methods and estimators. During the Bayesian optimization hyperparameter tuning in Step 4, the number of samples ranged from 1 to 50, selected as appropriate depending on the number and range of estimator hyperparameters.

We evaluated several clinically accessible input features for each prediction task to search for the best performing combinations. The input features were divided a priori into three feature blocks: *Clinical Variables* ($n_{\text{features}} = 7$), *Plasma Variables* ($n_{\text{features}} = 6$), and *MRI Variables* ($n_{\text{features}} = 247$). Clinical variables were basic demographics (age, sex, education level, number of apolipoprotein E [*APOE*] ε2 alleles, and number of *APOE* ε4 alleles) as well as two cognitive tests (Mini-Mental State Examination [MMSE] and delayed 10-word recall). Plasma biomarkers were p-tau217, p-tau181, p-tau231, e NTA, GFAP, and NfL. Structural MRI features included FreeSurfer volumes, surface areas and thicknesses of cortical regions, volumes of subcortical brain regions, total white matter hyperintensities (WMHIs), and total intracranial volume (ICV). An overview of the correlation between all input features is displayed as a hierarchically clustered heatmap in Figure S2, with numerical details in the Supplementary Information (Feature Correlation Matrix). The three input feature blocks *Clinical*, *Plasma* and *MRI Variables* were analyzed separately or together in all possible combinations (seven in total); see Figure 2.

## 2.7 | SHAP analysis

SHapley Additive exPlanations (SHAP) is a method developed by Lundberg et al. for model output explanation, originating from game theory.[44] It utilizes the Shapley values, which is a measure of how much each feature $x$ contributes to the final prediction $f(x)$, taking interaction effects between features into account (since certain permutations can make features contribute more than the sum of their parts). A local explanatory linear model

$$g\left(x'\right) = \phi_0 + \sum_{i=1}^{M} \phi_i x_i' \tag{2}$$

is created that converges to the original model $f(x)$ when $x' \approx x$, where $x'$ are simplified input features (binary inclusion/exclusion of a feature), $\phi_0$ is the model output with all input features missing, and Shapley values $\phi$ are the coefficients.

15525279, 2025, 2, Downloaded from https://alz-journals.onlinelibrary.wiley.com/doi/10.1002/alz.14600, Wiley Online Library on [11/08/2025]. See the Terms and Conditions (https://onlinelibrary.wiley.com/terms-and-conditions) on Wiley Online Library for rules of use; OA articles are governed by the applicable Creative Commons License

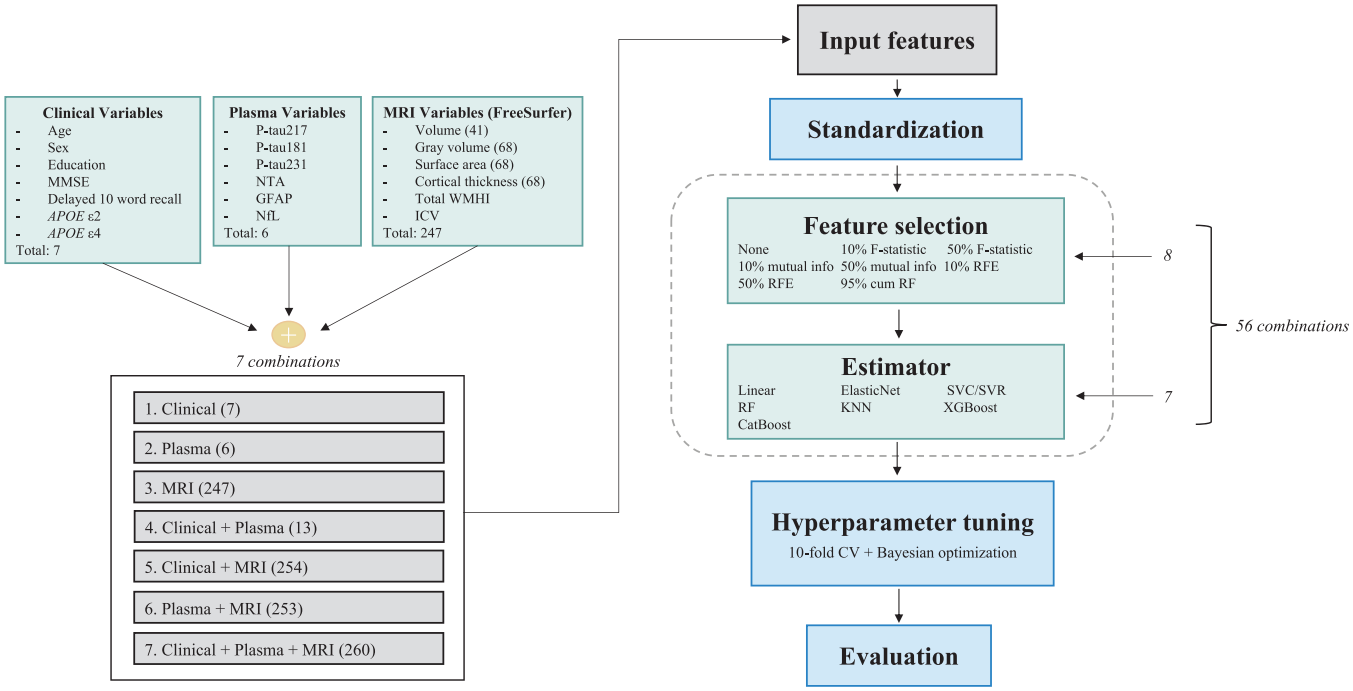


**FIGURE 2** A rigorous and flexible ML pipeline created to compare combinations of input features in regression and classification tasks. Three different blocks of variables (clinical, plasma, and MRI) were tested separately and in combination as input features in a pipeline created to search for high-performing ML models for regression and classification tasks. The pipeline consisted of a combined grid search (feature selection and estimators, in total 56 combinations) and Bayesian optimization (hyperparameter tuning, in a 10-fold cross-validations setting) approach with the best score, corresponding tuned hyperparameters, and computational times for all 56 combinations as output. The pipeline could handle different input and output variables, evaluation metrics, and both regression and classification tasks, making it applicable to any such ML task. Code was written in Python and is available on https://github.com/DeMONLab-BioFINDER/karlsson-predict-taupet. CV, cross validation; ICV, intracranial volume; KNN, K-nearest neighbor; cum RF, cumulative random forest feature importance; ML, machine learning; MMSE, Mini-Mental State Examination; MRI, magnetic resonance imaging; SVC/SVR, support vector classifier/regressor; RF, random forest; RFE, recursive feature elimination; WMHIs, white matter hyperintensities; APOE, Apolipoprotein E; p-tau, phosphorylated-tau; NTA, N-terminal containing tau fragments; GFAP, glial fibrillary acidic protein; NfL, neurofilament light.

## 2.8 | Statistical analysis

The BF2 participants were split randomly into an 80% training set ($n$ = 948) and 20% test set ($n$ = 247). Search for hyperparameter-tuned high-performing ML models was performed using 10-fold cross-validation within the training data set. The best model was thereafter evaluated on new unseen data; the left-out BF2 test data set; and the external test data sets BF1, ADNI, OASIS3, A4, and UCSF-ADRC. Note that the relevant plasma variables were not available to us in OASIS3 and A4, preventing external validation for all models using plasma in these cohorts.

For two-step classification, Step 1 was trained using the BF2 training set and Step 2 was trained using tau-PET-positive individuals from the BF2 training set, OASIS3, and A4. The BF2 test, BF1, ADNI, and UCSF-ADRC were used to test both steps, with only the predicted tau-PET-positive individuals from Step 1 evaluated in Step 2 for an as realistic a simulation as possible. Regression models were optimized on MSE and classification models on accuracy. Details on feature selection methods, estimators, and metrics can be seen in Table S2. One-tailed significance testing was performed as bootstrapped difference for a given metric between models. $p$-values were adjusted for multiple comparisons by the Benjamini–Hochberg false discovery rate (FDR) method.

## 2.9 | Imputation and missing data

For fair comparison of performance between the different input feature blocks, only participants with complete data for all clinical, plasma, and MRI variables were included from BF2. However, no other cohort included the full set of variables available in BF2, so some variables were imputed using a K-nearest neighbor (KNN) imputer (trained with the training set, number of neighbors = 5) to make the external evaluation possible. Note that if a missing variable was a main contributor during the prediction (assessed in the SHAP analysis), the cohort was not considered sufficient for testing (e.g., as A4 and OASIS3 were missing plasma p-tau217 they were excluded when predicting temporal lobe tau load). See Table S3 for details on variable imputations for each cohort.

15525279, 2025, 2, Downloaded from https://alz-journals.onlinelibrary.wiley.com/doi/10.1002/alz.14600, Wiley Online Library on [11/08/2025]. See the Terms and Conditions (https://onlinelibrary.wiley.com/terms-and-conditions) on Wiley Online Library for rules of use; OA articles are governed by the applicable Creative Commons License

### 2.10 | Computational resources

The 56 feature selection + estimator combinations in the ML pipeline were parallelized for time efficiency. Computations were performed on the Bianca Cluster, which is a part the National Academic Infrastructure for Supercomputing in Sweden (NAISS). Bianca is dedicated to analyses of sensitive data, providing 4480 cores in the form of 204 dual CPU (Intel Xeon E5-2630 v3) Huawei XH620 V3 nodes with 128 GB memory.

## 3 | RESULTS

### 3.1 | Plasma biomarkers were superior for predicting the load of temporal lobe tau tangle pathology

The first tau-PET outcome we assessed was continuous Braak I-IV tau load (i.e., SUVR in the commonly used temporal meta-ROI). The *Plasma Variables* feature block consistently produced the lowest MSE, both alone and in combination with the other feature blocks (Figure 3A). Tree-based ML models (RF and boosting regressors) were superior to linear, elastic net, and KNN for most feature combinations. Details on MSE, selected hyperparameters, and computational times for all 56 combinations in the ML pipeline and every input feature block can be seen in the Supplementary Information (ML output tau-PET load).

For each of the seven combinations of feature inputs, the best model (lowest MSE in Figure 3A and Table S4) was selected for further evaluation in the BF2 test set and external cohorts BF1, ADNI, and UCSF-ADRC (note that OASIS and A4 were excluded from this part due to absence of plasma variables). Performance on the BF2 test set, BF1, and other external cohorts was similar to the corresponding cross-validated training set performance (Figure 3B and Table S5). The best model in the cross-validated training set was a boosting regressor (CatBoost model) that from clinical, plasma, and MRI utilized a 95% cumulative RF feature selection (R-squared = 0.72 and mean absolute error [MAE] = 0.15 SUVR). On unseen test/external data, it resulted in R-squared of 0.66–0.69 and MAE of 0.16–0.17 SUVR, indicating high generalizability. However, other feature combinations that included plasma variables but not MRI and/or clinical variables reached similar or even higher performance on the test data sets (Figure 3B and Table S5), highlighting how fluid biomarkers were the key attribute to predict tau load. This was also visible in scatter plots of the true versus predicted results from the best model for each feature block combination (Figure 3C). Using just clinical variables resulted in limited predicted value (R-squared = 0.30–0.38). Using just MRI variables resulted in some predictive value but models tended to underestimate tau load (R-squared = 0.46–0.53). Adding clinical or MRI information to the plasma biomarker block led to only marginal improvement. We did not observe any systematical difference in the performance of the ML models for White and non-White participants (Figure S3A).

Because many models within each feature block performed very similar in the BF2 training set (Figure 3A), we investigated if this small MSE difference affected the ability of the model to generalize to unseen data. We compared the best five models within each input block combination (Table S5 and Figure S4). The top five models performed similarly within each feature block, but the distinction between input feature blocks remained such that inclusion of plasma biomarkers always resulted in the best predictive performance.

As the outcome variable was imbalanced between low and high load cases, we stratified the evaluation based on diagnostic groups. In this way, the evaluation metric would be more representative of the varying performance along the distribution of tau-PET load. Predicting tau-PET load was easiest for cognitively unimpaired (CU) and mild cognitively impaired (MCI) participants with no to moderate tau-PET load (lowest error in Figure 3E). Plasma variables yielded superior results in all diagnostic groups but stood out the most by accurately identifying low tau load in the non-AD dementia group (Figure 3E). Clinical (e.g., cognitive tests and basic demographics) and MRI variables were less efficient when differentiating neurodegeneration due to tau pathology versus another pathology (larger errors for other dementias and mild cognitive impairment [MCI]). In the AD dementia group, adding clinical and MRI variables to plasma improved performance slightly, but at the expense of inferior performance in other dementias. We saw no improved performance in predicting tau-PET load in A$\beta$-positive individuals when re-running the pipeline after excluding all A$\beta$-negative individuals, suggesting that the large proportion of participants with low tau load did not impair the models' predictive ability of participants with high tau load.

SHAP analysis was used to interpret which features contributed most to the prediction. This analysis showed that plasma p-tau217 was clearly the most important predictor of temporal tau-PET load (Figure 3D). Plasma p-tau217 contributed more to predictions when it had higher concentrations (higher feature value in the Figure 3D). For further model transparency, the SHAP interaction plots for the features in Figure 3D are provided in Figure S5.

Because plasma p-tau217 alone stood out as the most informative during the prediction of tau-PET load, we compared the best ML models against a simple linear regression model using only p-tau217 as a predictor. ML models without any plasma variables usually performed worse than the simple plasma p-tau217 linear model. Models combining the plasma feature block with clinical and/or MRI variables provided significantly better predictive performance than the simple model for the BF2 test set ($\Delta$R-squared = 0.13–0.18, $\Delta$MAE = 0.031–0.039 SUVR) and for the external cohorts UCSF-ADRC and ADNI ($\Delta$R-squared = 0.10–0.18, $\Delta$MAE = 0.025–0.050 SUVR). In BF1, only the "fluid + clinical" model significantly outperformed the plasma p-tau217 model, and only regarding MAE ($\Delta$MAE = 0.030 SUVR). All results are listed in Table S6.

### 3.2 | MRI features contain spatial information predictive of asymmetric tau load

The second tau-PET outcome we assessed in this work was asymmetry in tau load between the two hemispheres, that is, a Braak I-IV LI,

15525279, 2025, 2, Downloaded from https://alz-journals.onlinelibrary.wiley.com/doi/10.1002/alz.14600, Wiley Online Library on [11/08/2025]. See the Terms and Conditions (https://onlinelibrary.wiley.com/terms-and-conditions) on Wiley Online Library for rules of use; OA articles are governed by the applicable Creative Commons License

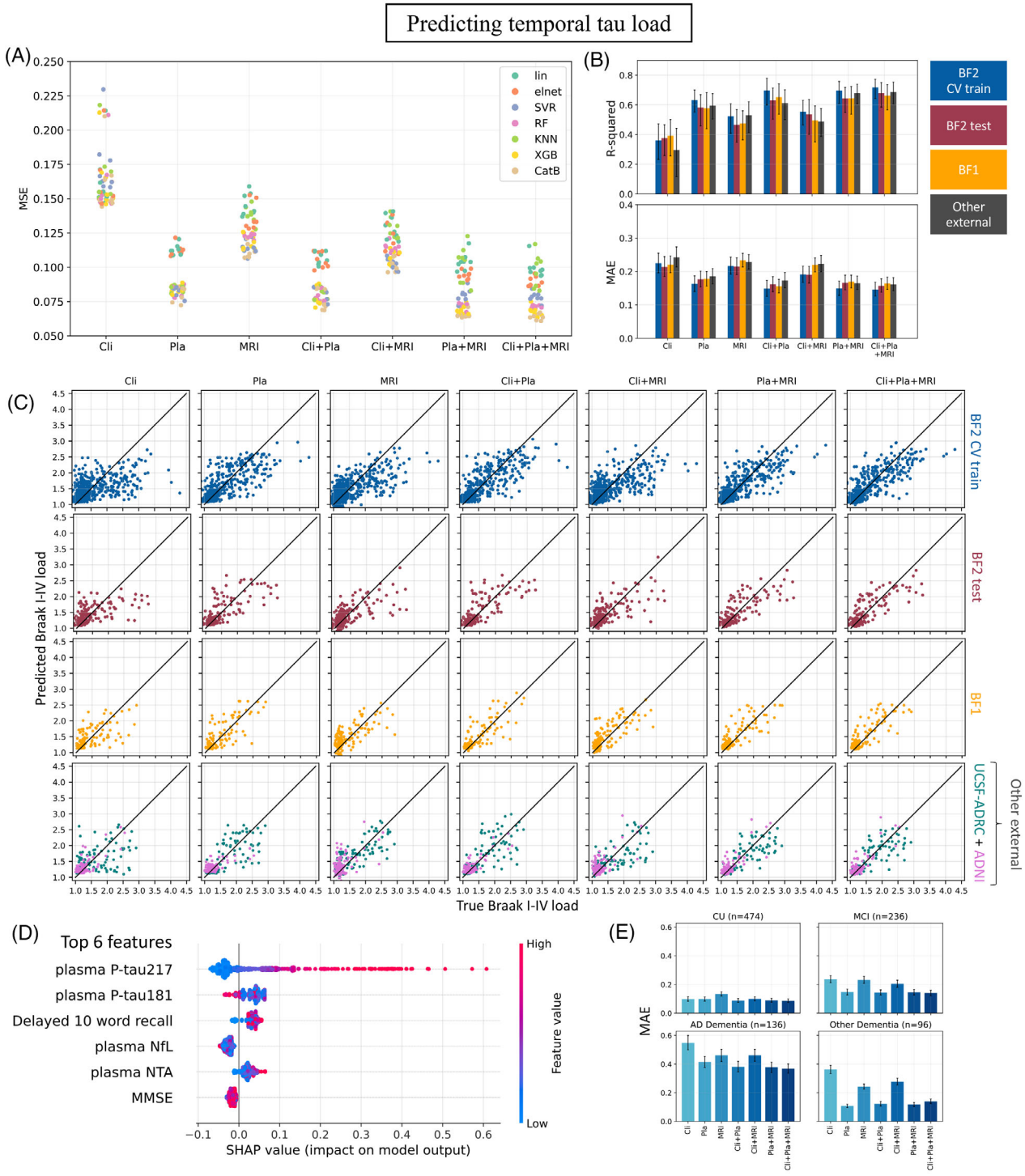


**FIGURE 3** Plasma features were most predictive of temporal tau load. (A) Mean squared error (MSE) of all 56 feature selection + estimator combinations (Figure 2) for the different input feature blocks (clinical, plasma, MRI, and all combinations) when predicting temporal tau load in the cross-validated BF2 training set. Each scatter point is colored by estimator. The blocks that included plasma features consistently performed best, always in a CatBoost model. (B) R-squared and mean absolute error (MAE) of the best pipeline combinations in (A) for the cross-validated BF2 training set, BF2 test set, and external test cohorts BF1, ADNI, and UCSF-ADRC. (C) Scatter plots of true versus predicted Braak I-IV (temporal tau) load for the best pipeline combinations in (A) for the cross-validated BF2 training set, BF2 test set, BF1, ADNI, and UCSF-ADRC. (D) Top SHAP feature contributions in the model including all features, evaluated on the cross-validated BF2 training set. (E) MAE performance of best pipeline combination in (A) stratified by cognitive status in the cross-validated BF2 training set. AD, Alzheimer's disease; Cli, clinical; CatB, CatBoost regressor; CU, cognitively unimpaired; elnet, elastic net regressor; KNN, K-nearest neighbor regressor; lin, linear regressor; MAE, mean absolute error; MSE, mean squared error; MCI, mild cognitive impairment; MMSE, mini mental state examination NfL, neurofilament light; NTA, N-terminal containing tau fragments; Pla, plasma; p-tau, phosphorylated tau; RF, random forest regressor; SVR, support vector regressor; XGB, XGBoost regressor.

15525279, 2025, 2, Downloaded from https://alz-journals.onlinelibrary.wiley.com/doi/10.1002/alz.14600, Wiley Online Library on [11/08/2025]. See the Terms and Conditions (https://onlinelibrary.wiley.com/terms-and-conditions) on Wiley Online Library for rules of use; OA articles are governed by the applicable Creative Commons License

specifically in tau-positive participants (assessed with tau-PET). For this task, the *MRI Variables* consistently produced the lowest MSE, both alone and in combination with the other feature blocks (Figure 4A). Support vector regressor (SVR) models resulted in best performance, followed by tree-based (RF and boosting) and elastic net regressors. Details on all 56 combinations and input feature blocks in the ML pipeline can be seen in the Supplementary Information (ML output tau-PET asymmetry).

The best model for each feature input block (lowest MSE in Figure 4A, details in Table S4) was evaluated in the BF2 test set and external cohorts BF1, ADNI, UCSF-ADRC, OASIS3, and A4. Combinations with plasma were evaluated only in BF2 and BF1. R-squared and MAE values varied between cohorts (Figure 4B and Tables S7 and S8), but combinations including the MRI variable block consistently resulted in the best performance (R-squared = 0.28–0.42 and MAE = 6.7–9.6 LI). The prediction results are presented in scatter plots, revealing high/consistent generalizability (Figure 4C). We did not observe any systematical difference in performance of the ML models for White and non-White participants (Figure S3B).

We next compared the top five models within each input block combinations to further explore generalization properties (Table S7 and Figure S6). The best five models had small variation within input feature blocks for both the BF2 test set and BF1 cohort. No obvious differences in model performance were seen across the five best models within an input feature block. Models including MRI features invariably outperformed models without these features.

SHAP analysis revealed that the most predictive features of tau-PET temporal lobe laterality were temporal lobe MRI gray matter volumes and cortical thicknesses (Figure 4D and 4E). Reasonably, the model inferred less gray matter in the left hemisphere as predictive of left-laterality, and vice versa (Figure 4D). For further model transparency, the SHAP interaction plots for the top six features in Figure 4D are provided in Figure S7.

We also evaluated two additional spatial measures of tau-PET: classification of tau-PET Subtype and Stage Inference (SuStaIn) subtypes[19] and regression of medial temporal lobe tau load versus cortical tau load. The analyses included smaller sample sizes and/or lower performances, but in both cases, ML models that include MRI variables consistently performed best (Supplementary Note 1).

### 3.3 | Proof-of-concept for a two-step model for clinical use

The translation of predictive models into clinically useful tools is an essential but often overlooked aspect of ML studies in AD. We combined the tasks from the previous two sections to create a two-step approach that can allow a clinician to simultaneously evaluate a patient's tau-PET load and laterality. First, plasma biomarkers would be used to assess if a patient is tau-PET positive. Second, in those classified as tau-PET positive by the blood biomarkers, an MRI-based algorithm is applied to assess whether the tau pattern is likely to be symmetric or whether tau load is higher in the left or right hemisphere. We reformulated the tasks into classification instead of regression, since categorical outcomes often are clearer and easier to interpret, which are important factors in a clinical context.

We simulated such a clinical scenario with a two-step classification task of predicting: (1) the two-label classification task of tau-PET positivity/negativity using plasma variables, and if tau-positive: (2) the three-label classification task of a left-asymmetric/right-asymmetric/symmetric tau phenotype using MRI variables. For this, the ML pipeline was re-run to search for the best-performing ML classifiers (note that in the previous sections the estimators were optimized for regression and not classification tasks), which thereafter were evaluated on unseen data using the BF2 test set and BF1. The proposed workflow and results are visualized in Figure 5, revealing accuracies between 0.86 and 0.92 for Step 1 (predicting tau positivity, two-label task) using an XGBoost model and promising performance (accuracy 0.61–0.65) for Task 2 (predicting tau laterality, three-label task) using an XGBoost model. This can be further compared against a model always predicting the majority class, which would have yielded an accuracy of 0.65–0.78 for Step 1, and 0.42–0.45 for Step 2, based on the class distributions in the test cohorts. Note, however, that when dichotomizing the tau-PET load outcome variable (and thereby reducing its variability), a simple logistic regression model with only plasma p-tau217 as input performed similarly to the best ML models (no significant differences in BF2 cross-validated training set, BF2 test set, BF1, ADNI, or UCSF-ADRC). Also note that when reducing the laterality classification to a two-label task of predicting more left or right temporal tau (indicated by a negative or positive LI), accuracies of 0.70–0.87 and areas under the curve (AUCs) of 0.76–0.93 were achieved (Figure S8). This highlights the ML models' ability to capture spatial tau-PET information with promising performance.

Two other potential workflows were also tested: using "clinical + plasma + MRI" variables as input for both steps and using "only MRI" for both steps. The workflow including all feature input blocks performed similar to using plasma variables for Task 1 and MRI variables for Task 2 (Task 1 accuracy: 0.84–0.93, Task 2 accuracy: 0.53–0.63), whereas the "MRI only" workflow performed slightly inferior (Task 1 accuracy: 0.82–0.89, Task 2 accuracy: 0.46–0.58). See Tables S9 and S10 for details on all workflows.

## 4 | DISCUSSION

We address the issue of limited access to tau-PET by investigating the utility of various ML models and readily available data (clinical, plasma, and structural MRI) to predict important information from tau-PET. We formulated two regression tasks: predicting tau-PET SUVR in the temporal lobe and predicting hemispheric asymmetry of temporal lobe tau load in tau-positive participants. We implemented a rigorous ML pipeline that searched for high-performing combinations of feature selection steps and estimators in a combined grid-search and Bayesian optimization set-up. Plasma features (particularly plasma p-tau217) resulted in the best prediction of temporal lobe tau SUVR, whereas MRI features resulted in the best prediction of temporal lobe

15525279, 2025, 2, Downloaded from https://alz-journals.onlinelibrary.wiley.com/doi/10.1002/alz.14600, Wiley Online Library on [11/08/2025]. See the Terms and Conditions (https://onlinelibrary.wiley.com/terms-and-conditions) on Wiley Online Library for rules of use; OA articles are governed by the applicable Creative Commons License

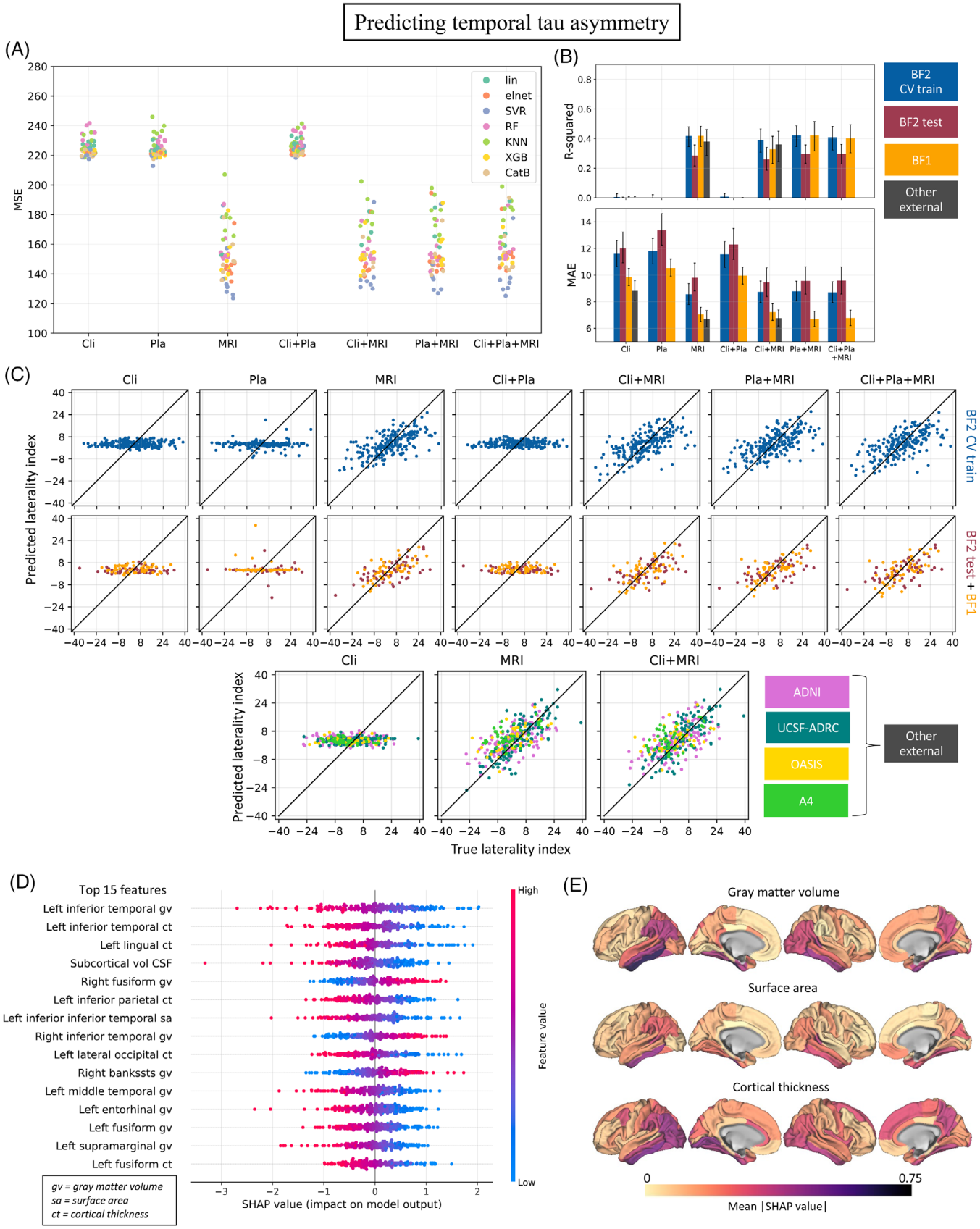


**FIGURE 4** MRI features were most predictive of temporal hemispheric tau asymmetry. (A) Mean squared error (MSE) of all 56 feature selection + estimator combinations (Figure 2) for the different input feature blocks (clinical, plasma, MRI, and all combinations) when predicting tau-PET asymmetry in the cross-validated BF2 training set. Each scatter point is colored by estimator. The blocks that included MRI features

15525279, 2025, 2, Downloaded from https://alz-journals.onlinelibrary.wiley.com/doi/10.1002/alz.14600, Wiley Online Library on [11/08/2025]. See the Terms and Conditions (https://onlinelibrary.wiley.com/terms-and-conditions) on Wiley Online Library for rules of use; OA articles are governed by the applicable Creative Commons License

tau asymmetry. The models were evaluated on unseen test data and independent cohorts, revealing a high degree of model generalizability. We also simulated a two-step model for clinical use, which showed promising performance in classifying tau-PET positivity and spatial asymmetry from plasma and MRI variables, but still requiring improvement before suitable to apply in a clinical setting. This study highlights the current potential in predicting tau-PET from more accessible variables, which could dramatically improve diagnosis and prognosis of AD by using scalable, cost-effective methods.

Overcoming the high cost of tau-PET is an important challenge in AD research. Tau-PET has been shown to add clinical information beyond fluid biomarkers, increasing the diagnostic confidence of treating clinicians.[45] It is also used as a screening tool and to monitor treatment effects in clinical trials.[10,12] Furthermore, results from the TRAILBLAZER-ALZ 2 Randomized Clinical Trial have suggested that the amyloid-lowering therapy donanemab provided a greater benefit when initiated at an earlier disease stage (as was indicated by less tau accumulation using tau-PET).[46] Early therapeutic intervention has also previously been highlighted as key for a more meaningful disease modification in AD.[47,48] This emphasizes the importance of broad tau-PET accessibility to increase diagnostic confidence, reduce costs in clinical trials, and enable effective early treatment in a large population.

Here, we approach this problem with ML models, highlighting the potential in combining plasma and MRI features to predict both temporal lobe tau load and spatial patterns. These implications are informative for future studies aimed to improve predictions of tau-PET from more accessible data, for example, in studies aimed to synthesize full tau-PET scans using more advanced mathematical models (e.g., deep learning). Such attempts have been made already, but usually high performance has only been reached when using other PET modalities, and thereby not removing the need of a PET scan in the AD diagnostic workflow. Lee et al. were, for example, able to synthesize tau-PET scans with high accuracy using fluorodeoxyglucose (FDG) and amyloid PET, but saw notably inferior performance when using MRI.[49] Chen et al. showed that full-dose PET images may be predicted from MRI and ultra-low-dose tau-PET images in deep learning models, reducing the radiation but still requiring a PET scan.[50] Results of our study highlight that combining plasma biomarkers and MRI can be a potential way forward in synthesizing full tau-PET scans without requiring any kind of PET modality as input.

Plasma biomarkers are not yet broadly available, but due to their low cost and high accuracy, they are likely to play an important role in future AD diagnostics. Recent work has successfully evaluated them in primary care, highlighting their potential for broad clinical use.[51] The relationship between plasma biomarkers and tau-PET load has been examined extensively in research studies, but often with dichotomous tau-PET load rather than continuous as outcome, in inferential settings rather than predictive, and mainly looking at linear associations rather than more complex relationships within the data.[12] Nonetheless, plasma p-tau217 often shows a superior association with temporal lobe tau load compared to other plasma biomarkers (including other p-tau species),[13,25,36,52–54] and even reaches equal or superior performance compared to CSF biomarkers.[55] This is in line with our results, highlighting the dominant contribution from plasma p-tau217 in predicting temporal lobe tau load at different stages of the disease, even when other variables associated with tau burden also were available. Devanarayan et al. similarly found plasma p-tau217 to better predict continuous tau accumulation in several brain regions compared to clinical assessments, MRI, and other plasma biomarkers.[56]

Not only did plasma p-tau217 stand out as the main contributing feature in the best ML model, but a linear regression model with only plasma p-tau217 usually outperformed more complex ML models trained without plasma features. Plasma p-tau217 has also been shown efficient when differentiating AD dementia from other neurodegenerative diseases,[25,36,57] in line with the results presented in Figure 3E. This stratified evaluation suggested that there was little to no gain from adding clinical and MRI variables to a model with only plasma variables in a setting where other neurodegenerative diseases are present (e.g., in primary care or at a memory clinic), as these added variables did not differentiate well between pathological changes due to AD dementia or other dementias. Within the AD dementia group, however, a small improvement was seen when adding the clinical and MRI variables, indicating that these features potentially could add more predictive information in a setting where cognitive impairment is very likely due to AD (e.g., a clinical trial). Note that the included clinical variables were aimed to represent highly accessible features, and therefore, relatively broadly used and readily administered cognitive tests were selected. More comprehensive or sophisticated cognitive evaluations may improve the differentiation between dementias. Furthermore, plasma p-tau217 has been suggested to relate both to tau and amyloid load in AD.[58] Upcoming, more tau pathology–specific fluid-based biomarkers (e.g., microtubule-binding region of tau MTBR-tau243[59]), as well as enhancement of plasma p-tau217 by, for example, normalizing it to non-phosphorylated tau-217,[56] can likely improve tau-PET prediction even further.

MRI models consistently underestimated the amount of tau in the brain. This may be related to the fact that neurodegeneration measurable with MRI likely occurs after tau has already infiltrated a brain region.[60] It may also be related to differences in resilience to tau load, as some individuals may be able to harbor tau for long without experi-

consistently performed best, always in an SVR model. (B) R-squared and mean absolute error (MAE) of best pipeline combinations in (A) for the cross-validated BF2 training set, BF2 test set, and external test cohorts BF1, ADNI, UCSF-ADRC, OASIS3, and A4. (C) Scatter plots of true versus predicted laterality index for the best pipeline combinations in (A) for the cross-validated BF2 training set and test set, and the other external cohorts. (D) top SHAP feature contributions in the model including all features, evaluated on the cross-validated BF2 training set. (E) visualization of the SHAP feature contribution analysis for the MRI FreeSurfer variables. Cli, Clinical; CatB, CatBoost regressor; elnet, elastic net regressor; KNN, K-nearest neighbor regressor; lin, linear regressor; MAE, mean absolute error; MSE, mean squared error; Pla, Plasma; RF, random forest regressor; SVR, support vector regressor; XGB, XGBoost regressor.

15525279, 2025, 2, Downloaded from https://alz-journals.onlinelibrary.wiley.com/doi/10.1002/alz.14600, Wiley Online Library on [11/08/2025]. See the Terms and Conditions (https://onlinelibrary.wiley.com/terms-and-conditions) on Wiley Online Library for rules of use; OA articles are governed by the applicable Creative Commons License

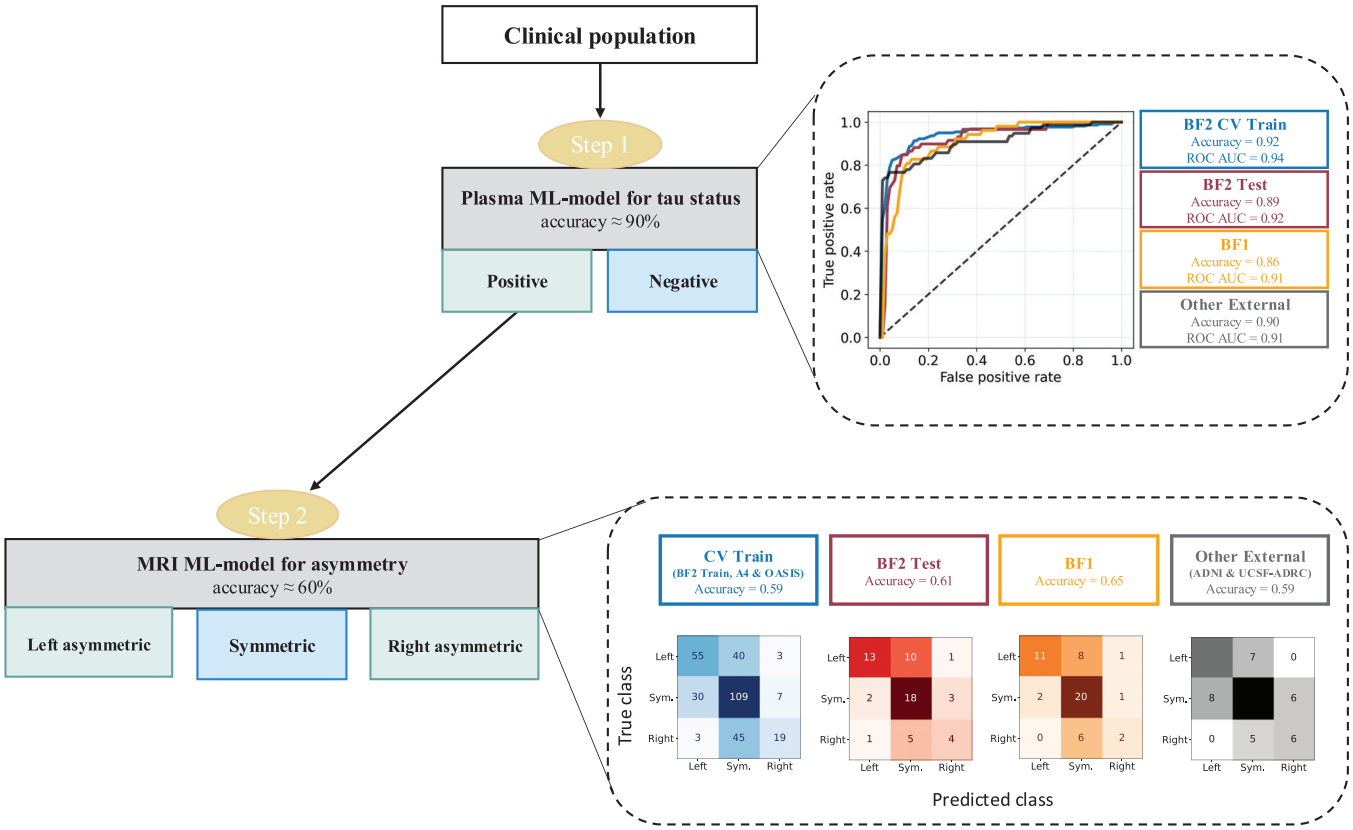


**FIGURE 5** A simulated two-step classification scenario predicting (1) tau-positivity/negativity (load) using plasma variables and if tau-positive: (2) left-asymmetric/symmetric/right-asymmetric using MRI variables. Step 1 was trained on the full BF2 training set, and Step 2 on tau-PET positive participants from BF2 training set, OASIS3, and A4. Results were evaluated on the cross-validated training set (blue), BF2 test set (red), and external cohorts BF1 (orange), ADNI and UCSF-ADRC (gray). Note that for Step 2, the training set contained true tau-PET positive participants, whereas the test sets included predicted positive participants from Step 1.

encing atrophy.[61–63] Moreover, soluble tau phosphorylation patterns detected by plasma provided no predictive information of lateralization in tau load. This may provide some limited evidence against the idea of the hemispheric lateralization being related to differences in the biochemistry of tau. Potential other mechanisms, like, for example, differences in brain connectivity or genomic factors, could instead be possible underlying causes of varying lateralization patterns,[64] but this should be further explored in future works.

We proposed a potential two-step clinical platform, which could be of utility in a clinical population where tau-PET currently is not available. Tau-PET positivity is a well-established marker of the pathological process of AD,[2] and analyzing spatial tau accumulation patterns allows for more detailed patient-specific evaluations, can improve diagnostic certainties, and influence changes in medication.[19,45] Temporal lobe tau laterality has more specifically been suggested to influence behavior and language patterns in AD,[24] and be linked to faster AD progression,[19] indicating that information on tau-PET asymmetry may improve AD prognoses in an individualized manner. Here, tau positivity was first classified and, if positive, a laterality class of symmetric, left asymmetric, or right asymmetric was also predicted. The first classifier was able to discriminate tau-PET-positive from tau-PET-negative participants with ≈90% accuracy. The second classifier had an accuracy of ≈60%, which can be regarded promising considering that this was a multi-label task (always predicting the majority class would result in ≈40% accuracy). This two-step approach still requires improvement before it is suitable to apply in a clinical setting due to the limited performance. This might be achieved in future studies that, for example, train ML models on larger samples and include more tau-specific plasma biomarkers (e.g., MTBR-tau243).

The evaluation metrics in this work are well established within the field of ML and are clearly representative of model performance within a cohort. However, when the outcome variable is imbalanced or unequally represented at different parts of the distribution, evaluation metrics can be highly sensitive to cohort properties, potentially influencing the interpretation of model generalizability. When predicting tau-PET asymmetry, lower MAE was, for example, obtained in the external cohorts compared to the cross-validated BF2 (Figure 4). Usually ML models are expected to perform similar or worse on external data, as the model unlikely has learned characteristics that are not present in the training set. However, since the external cohorts in this work had a narrower LI distribution with fewer extreme left/right asymmetric cases (as seen in Figure 1), the prediction task becomes easier, which may explain the better performance according to the MAE metric. Furthermore, when predicting tau-PET load

15525279, 2025, 2, Downloaded from https://alz-journals.onlinelibrary.wiley.com/doi/10.1002/alz.14600, Wiley Online Library on [11/08/2025]. See the Terms and Conditions (https://onlinelibrary.wiley.com/terms-and-conditions) on Wiley Online Library for rules of use; OA articles are governed by the applicable Creative Commons License

(Figure 3C), the majority of individuals in all cohorts had relatively low tau load and therefore covered a small range of the outcome variable distribution. The expected absolute value of the error hence increased for higher true tau load cases, often making it more informative to compare model performance between cohorts by looking at the scatter plots (Figure 3C) and/or stratify by diagnostic groups (as was done in Figure 3E). These results revealed that to improve the models further, additional refinement when predicting load in individuals within the tau-PET positive range is of main importance. This could likely be achieved through larger sample sizes, more tau-specific fluid biomarkers (e.g., MTBR-tau243), and/or more advanced modeling methods.

Limitations of this study include the varying overlap of data between cohorts, for example, hindering us to evaluate the performance of plasma biomarkers in all external cohorts. Furthermore, the predictive performance of ML estimators is always highly dependent on the data distribution and structures within the available training data. In addition, demographic biases in the data existed, for example, mainly highly educated, white participants. Future work is needed to assess generalizability to a more diverse population, as the proportion of non-White individuals was small in this study. Nevertheless, this work explores a promising approach to perform tau-PET prediction by incorporating multiple levels of data in ML models. Our study highlights both promising and limiting aspects of several clinically accessible variables in this context, with broad relevance for clinical settings and future research.

## ACKNOWLEDGMENTS

The authors would like to express our gratitude to the research volunteers who participated in the studies from which these data were obtained, as well as to their supportive families.

All protocols were approved by each cohort's respective institutional ethical review board, and all participants gave written informed consent.

## CONFLICT OF INTEREST STATEMENT

O.H. is a part-time employee of Eli Lilly and Lund University, and he has previously acquired research support (for Lund University) from AVID Radiopharmaceuticals, Biogen, C2N Diagnostics, Eli Lilly, Eisai, Fujirebio, GE Healthcare, and Roche. In the past 2 years, he has received consultancy/speaker fees from Alzpath, BioArctic, Biogen, Bristol Meyer Squibb, Eisai, Eli Lilly, Fujirebio, Merck, Novartis, Novo Nordisk, Roche, Sanofi, and Siemens. R.S. has received speaker's fees from Roche. H.Z. has served on scientific advisory boards and/or as a consultant for Abbvie, Acumen, Alector, Alzinova, ALZPath, Amylyx, Annexon, Apellis, Artery Therapeutics, AZTherapies, Cognito Therapeutics, CogRx, Denali, Eisai, Merry Life, Nervgen, Novo Nordisk, Optoceutics, Passage Bio, Pinteon Therapeutics, Prothena, Red Abbey Labs, reMYND, Roche, Samumed, Siemens Healthineers, Triplet Therapeutics, and Wave; has given lectures in symposia sponsored by Alzecure, Biogen, Cellectricon, Fujirebio, Lilly, Novo Nordisk, and Roche; and is a co-founder of Brain Biomarker Solutions in Gothenburg AB (BBS), which is a part of the GU Ventures Incubator Program (outside submitted work). K.B. has served as a consultant and on advisory boards for Abbvie, AC Immune, ALZPath, AriBio, BioArctic, Biogen, Eisai, Lilly, Moleac Pte. Ltd, Neurimmune, Novartis, Ono Pharma, Prothena, Roche Diagnostics, and Siemens Healthineers; has served on data-monitoring committees for Julius Clinical and Novartis; has given lectures, produced educational materials, and participated in educational programs for AC Immune, Biogen, Celdara Medical, Eisai, and Roche Diagnostics; and is a co-founder of Brain Biomarker Solutions in Gothenburg AB (BBS), which is a part of the GU Ventures Incubator Program, outside the work presented in this article. J.S. and R.A.I.B. are directors of and hold equity in Centile Bioscience Inc. S.P. has acquired research support (for the institution) from ki elements/ADDF and Avid. In the past 2 years, he has received consultancy/speaker's fees from BioArctic, Biogen, Esai, Lilly, and Roche. R.O. has received research funding/support from European Research Council, ZonMw, NWO, National Institutes of Health (NIH), Alzheimer's Association, Alzheimer Nederland, Stichting Dioraphte, Cure Alzheimer's fund, Health Holland, ERA PerMed, Alzheimerfonden, Hjarnfonden, Avid Radiopharmaceuticals, Janssen Research & Development, Roche, Quanterix, and Optina Diagnostics; has given lectures in symposia sponsored by GE Healthcare; is an advisory board member for Asceneuron; and is a steering committee member for Bristol Myers Squibb. All the aforementioned has been paid to the institutions. A.P.B. is supported by a postdoctoral fellowship from the Fonds de recherche en Santé Québec (298314). G.D. receives research support from the NIH, Alzheimer's Association, American College of Radiology, Rainwater Charitable Foundation, Avid Radiopharmaceuticals, GE Healthcare, Life Molecular Imaging, and Genentech. He has served as a paid consultant to Eli Lilly, Merck, and Johnson & Johnson. He is an Associate Editor for *JAMA Neurology*. The remaining authors declare no competing interests. Work at the Clinical Memory Research Unit, Lund University, was supported by the National Institute on Aging (NIA; R01AG083740), European Research Council (ADG-101096455), Alzheimer's Association (ZEN24-1069572, SG-23-1061717), GHR Foundation, Swedish Research Council (2022-00775, 2021-02219, 2018-02052), ERA PerMed (ERAPERMED2021-184), Knut and Alice Wallenberg foundation (2022-0231), Strategic Research Area MultiPark (Multidisciplinary Research in Parkinson's Disease) at Lund University, Swedish Alzheimer Foundation (AF-980907, AF-994229), Swedish Brain Foundation (FO2021-0293, FO2023-0163), Parkinson Foundation of Sweden (1412/22), EU Joint Programme—Neurodegenerative Disease Research (2019-03401), WASP and DDLS Joint call for research projects (WASP/DDLS22-066), Cure Alzheimer's Fund, Rönström Family Foundation (FRS-0003), Konung Gustaf V:s och Drottning Victorias Frimurarestiftelse, Skåne University Hospital Foundation (2020-O000028), Regionalt Forskningsstöd (2022-1259), and Swedish federal government under the ALF agreement (2022-Projekt0080, 2022-Projekt0107). The precursor of $^{18}$F-flutemetamol was sponsored by GE Healthcare. The precursor of $^{18}$F-RO948 was provided by Roche. J.W.V. was supported by the SciLifeLab & Wallenberg Data Driven Life Science Program (grant: KAW 2020.0239), the Swedish Alzheimer Foundation, and the Crafoord Foundation. K.B. is supported by the Swedish Research Council (#2017-00915 and #2022-00732), the Swedish Alzheimer Foundation (#AF-930351, #AF-939721, #AF-

15525279, 2025, 2, Downloaded from https://alz-journals.onlinelibrary.wiley.com/doi/10.1002/alz.14600, Wiley Online Library on [11/08/2025]. See the Terms and Conditions (https://onlinelibrary.wiley.com/terms-and-conditions) on Wiley Online Library for rules of use; OA articles are governed by the applicable Creative Commons License

968270, and #AF-994551), Hjärnfonden, Sweden (#FO2017-0243 and #ALZ2022-0006), the Swedish state under the agreement between the Swedish government and the County Councils, the ALF-agreement (#ALFGBG-715986 and #ALFGBG-965240), the European Union Joint Program for Neurodegenerative Disorders (JPND2019-466-236), the Alzheimer's Association 2021 Zenith Award (ZEN-21-848495), the Alzheimer's Association 2022-2025 Grant (SG-23-1038904 QC), La Fondation Recherche Alzheimer (FRA), Paris, France, the Kirsten and Freddy Johansen Foundation, Copenhagen, Denmark, and Familjen Rönströms Stiftelse, Stockholm, Sweden. H.Z. is a Wallenberg Scholar and a Distinguished Professor at the Swedish Research Council supported by grants from the Swedish Research Council (#2023-00356; #2022-01018 and #2019-02397), the European Union's Horizon Europe research and innovation programme under grant agreement No 101053962, Swedish State Support for Clinical Research (#ALFGBG-71320), the Alzheimer Drug Discovery Foundation (ADDF), USA (#201809-2016862), the AD Strategic Fund and the Alzheimer's Association (#ADSF-21-831376-C, #ADSF-21-831381-C, #ADSF-21-831377-C, and #ADSF-24-1284328-C), the Bluefield Project, Cure Alzheimer's Fund, the Olav Thon Foundation, the Erling-Persson Family Foundation, Familjen Rönströms Stiftelse, Stiftelsen för Gamla Tjänarinnor, Hjärnfonden, Sweden (#FO2022-0270), the European Union's Horizon 2020 research and innovation programme under the Marie Skłodowska-Curie grant agreement No 860197 (MIRIADE), the European Union Joint Programme – Neurodegenerative Disease Research (JPND2021-00694), the National Institute for Health and Care Research University College London Hospitals Biomedical Research Centre, and the UK Dementia Research Institute at UCL (UKDRI-1003). K.B. is supported by the Swedish Research Council (#2017-00915 and #2022-00732), the Swedish Alzheimer Foundation (#AF-930351, #AF-939721, #AF-968270, and #AF-994551), Hjärnfonden, Sweden (#FO2017-0243 and #ALZ2022-0006), the Swedish state under the agreement between the Swedish government and the County Councils, the ALF-agreement (#ALFGBG-715986 and #ALFGBG-965240), the European Union Joint Program for Neurodegenerative Disorders (JPND2019-466-236), the Alzheimer's Association 2021 Zenith Award (ZEN-21-848495), the Alzheimer's Association 2022-2025 Grant (SG-23-1038904 QC), La Fondation Recherche Alzheimer (FRA), Paris, France, the Kirsten and Freddy Johansen Foundation, Copenhagen, Denmark, and Familjen Rönströms Stiftelse, Stockholm, Sweden. Data were provided in part by OASIS-3_AV1451: Principal Investigators: T. Benzinger, J. Morris; NIH P30 AG066444, AW00006993. UCSF data collection supported by ADRC NIH/NIA P30-AG062422 (G.D.R.), NIH/NIA R35 AG072362 (G.D.R.), and Rainwater Charitable Foundation (G.D.R.). AV-1451 doses were provided by Avid Radiopharmaceuticals, a wholly owned subsidiary of Eli Lilly. The computations were enabled by resources provided by the National Academic Infrastructure for Supercomputing in Sweden (NAISS) at Uppsala Multidisciplinary Center for Advanced Computational Science (UPPMAX), partially funded by the Swedish Research Council through grant agreement no. 2022-06725. The funding sources had no role in the design and conduct of the study; in the collection, analysis, interpretation of the data; or in the preparation, review, or approval of the manuscript. Author disclosures are available in the supporting information.

## DATA AVAILABILITY STATEMENT

Six different cohorts were used in this work: BF2, BF1, ADNI, UCSF-ADRC, A4, and OASIS3. ADNI, A4, and OASIS3 are publicly available data sets and can be obtained from http://adni.loni.usc.edu/, https://ida.loni.usc.edu/, and https://sites.wustl.edu/oasisbrains/, respectively. The other data sets are not publicly available, but pseudonymized data can be shared with qualified academic researchers upon request (for BF1 and BF2: contact the principal investigator O.H., for UCSF-ADRC: submit a request form at https://memory.ucsf.edu/research-trials/professional/open-science). For BF1 and BF2, data transfer must be performed in agreement with EU legislation regarding general data protection regulation and decisions by the Ethical Review Board of Sweden and Region Skåne.

## CODE AVAILABILITY

Code for the analyses can be found in the following GIT repository: https://github.com/DeMONLab-BioFINDER/karlsson-predict-taupet. All analyses were implemented using Python version 3.9. Python dependencies include NumPy,[65] pandas,[66] Matplotlib,[67] and Scikit-learn.[68] Note that the flexible ML pipeline is not specific to this work but can be applied for any classification/regression task with spreadsheet data.

## ORCID

*Linda Karlsson* https://orcid.org/0000-0002-0630-772X

## REFERENCES

1. Nichols E, Steinmetz JD, Vollset SE, et al. Estimation of the global prevalence of dementia in 2019 and forecasted prevalence in 2050: an analysis for the Global Burden of Disease Study 2019. *Lancet Public Health*. 2022;7:e105-25. doi:10.1016/S2468-2667(21)00249-8
2. Jack CR, Bennett DA, Blennow K, et al. NIA-AA Research Framework: toward a biological definition of Alzheimer's disease. *Alzheimer Dement*. 2018;14:535-562. doi:10.1016/j.jalz.2018.02.018
3. Hansson O. Biomarkers for neurodegenerative diseases. *Nat Med*. 2021;27:954-963. doi:10.1038/s41591-021-01382-x
4. Bao W, Xie F, Zuo C, Guan Y, Huang YH. PET Neuroimaging of Alzheimer's disease: radiotracers and their utility in clinical research. *Front Aging Neurosci*. 2021;13. doi:10.3389/fnagi.2021.624330
5. Ossenkoppele R, Rabinovici GD, Smith R, et al. Discriminative accuracy of [18F]flortaucipir positron emission tomography for Alzheimer disease vs other neurodegenerative disorders. *JAMA*. 2018;320:1151-1162. doi:10.1001/jama.2018.12917
6. Leuzy A, Smith R, Ossenkoppele R, et al. Diagnostic performance of RO948 F 18 tau positron emission tomography in the differentiation of alzheimer disease from other neurodegenerative disorders. *JAMA Neurol*. 2020;77:955-965. doi:10.1001/jamaneurol.2020.0989
7. Davatzikos C, Xu F, An Y, Fan Y, Resnick SM. Longitudinal progression of Alzheimers-like patterns of atrophy in normal older adults: the SPARE-AD index. *Brain*. 2009;132:2026-2035. doi:10.1093/brain/awp091
8. Schwarz CG, Gunter JL, Wiste HJ, et al. A large-scale comparison of cortical thickness and volume methods for measuring Alzheimer's disease severity. *Neuroimage Clin*. 2016;11:802-812. doi:10.1016/j.nicl.2016.05.017

15525279, 2025, 2, Downloaded from https://alz-journals.onlinelibrary.wiley.com/doi/10.1002/alz.14600, Wiley Online Library on [11/08/2025]. See the Terms and Conditions (https://onlinelibrary.wiley.com/terms-and-conditions) on Wiley Online Library for rules of use; OA articles are governed by the applicable Creative Commons License

9. van Dyck CH, Swanson CJ, Aisen P, et al. Lecanemab in early Alzheimer's disease. *N Engl J Med*. 2023;388. doi:10.1056/nejmoa2212948
10. Mintun MA, Lo AC, Duggan Evans C, et al. Donanemab in early Alzheimer's disease. *N Engl J Med*. 2021;384:1691-1704. doi:10.1056/NEJMoa2100708
11. Mummery CJ, Börjesson-Hanson A, Blackburn DJ, et al. Tau-targeting antisense oligonucleotide MAPTRx in mild Alzheimer's disease: a phase 1b, randomized, placebo-controlled trial. *Nat Med*. 2023;29:1437-1447. doi:10.1038/s41591-023-02326-3
12. Ossenkoppele R, van der Kant R, Hansson O. Tau biomarkers in Alzheimer's disease: towards implementation in clinical practice and trials. *Lancet Neurol*. 2022;21:726-734. doi:10.1016/S1474-4422(22)00168-5
13. Mattsson-Carlgren N, Collij LE, Stomrud E, et al. Plasma biomarker strategy for selecting patients with Alzheimer disease for antiamyloid immunotherapies. *JAMA Neurol*. 2024;81:69-78. doi:10.1001/jamaneurol.2023.4596
14. Ossenkoppele R, Pichet Binette A, Groot C, et al. Amyloid and tau PET-positive cognitively unimpaired individuals are at high risk for future cognitive decline. *Nat Med*. 2022;28:2381-2387. doi:10.1038/s41591-022-02049-x
15. Smith R, Cullen NC, Pichet Binette A, et al. Tau-PET is superior to phospho-tau when predicting cognitive decline in symptomatic AD patients. *Alzheimer Dement*. 2023;19:2497-2507. doi:10.1002/alz.12875
16. Ossenkoppele R, Smith R, Mattsson-Carlgren N, et al. Accuracy of Tau positron emission tomography as a prognostic marker in preclinical and prodromal Alzheimer disease: a head-to-head comparison against amyloid positron emission tomography and magnetic resonance imaging. *JAMA Neurol*. 2021;78:961-971. doi:10.1001/jamaneurol.2021.1858
17. Cho H, Choi JY, Hwang MS, et al. In vivo cortical spreading pattern of tau and amyloid in the Alzheimer disease spectrum. *Ann Neurol*. 2016;80:247-258. doi:10.1002/ana.24711
18. Pascoal TA, Therriault J, Benedet AL, et al. 18F-MK-6240 PET for early and late detection of neurofibrillary tangles. *Brain*. 2020;143:2818-2830. doi:10.1093/brain/awaa220
19. Vogel JW, Young AL, Oxtoby NP, et al. Four distinct trajectories of tau deposition identified in Alzheimer's disease. *Nat Med*. 2021;27:871-881. doi:10.1038/s41591-021-01309-6
20. Sarazin M, Lagarde J, Bottlaender M. Distinct tau PET imaging patterns in typical and atypical Alzheimer's disease. *Brain*. 2016;139:1321-1324. doi:10.1093/brain/aww041
21. Young CB, Winer JR, Younes K, et al. Divergent cortical Tau positron emission tomography patterns among patients with preclinical Alzheimer disease. *JAMA Neurol*. 2022;79:592-603. doi:10.1001/jamaneurol.2022.0676
22. Tetzloff KA, Graff-Radford J, Martin PR, et al. Regional distribution, asymmetry, and clinical correlates of Tau uptake on [18F]AV-1451 PET in atypical Alzheimer's disease. *J Alzheimer Dis*. 2018;62:1713-1724. doi:10.3233/JAD-170740
23. Martersteck A, Ayala I, Ohm DT, et al. Focal amyloid and asymmetric tau in an imaging-to-autopsy case of clinical primary progressive aphasia with Alzheimer disease neuropathology. *Acta Neuropathol Commun*. 2022;10:111. doi:10.1186/s40478-022-01412-w
24. Younes K, Smith V, Johns E, et al. Temporal tau asymmetry spectrum influences divergent behavior and language patterns in Alzheimer's disease. *Brain, Behavior and Immunity*. 2024;119:807-817. doi:10.1016/j.bbi.2024.05.002
25. Palmqvist S, Janelidze S, Quiroz YT, et al. Discriminative accuracy of plasma Phospho-tau217 for Alzheimer disease vs Other neurodegenerative disorders. *JAMA*. 2020;324:772-781. doi:10.1001/jama.2020.12134
26. Palmqvist S, Insel PS, Stomrud E, et al. Cerebrospinal fluid and plasma biomarker trajectories with increasing amyloid deposition in Alzheimer's disease. *EMBO Mol Med*. 2019;11:e11170. doi:10.15252/emmm.201911170
27. Tanner JA, Iaccarino L, Edwards L, et al. Amyloid, tau and metabolic PET correlates of cognition in early and late-onset Alzheimer's disease. *Brain*. 2022;145:4489-4505. doi:10.1093/brain/awac229
28. Thijssen E, Joie L, Strom AB, et al. Plasma phosphorylated tau 217 and phosphorylated tau 181 as biomarkers in Alzheimer's disease and frontotemporal lobar degeneration: a retrospective diagnostic performance study. *The Lancet Neurology*. 2021;20:739-752.
29. Sperling RA, Rentz DM, Johnson KA, et al. The A4 study: stopping AD before symptoms begin? *Sci Transl Med*. 2014;6. doi:10.1126/scitranslmed.3007941
30. Insel PS, Donohue MC, Sperling R, Hansson O, Mattsson-Carlgren N. The A4 study: $\beta$-amyloid and cognition in 4432 cognitively unimpaired adults. *Ann Clin Transl Neurol*. 2020;7:776-785. doi:10.1002/acn3.51048
31. Lamontagne PJ, Benzinger TLS, Morris JC, et al. OASIS-3: longitudinal neuroimaging, clinical, and cognitive dataset for normal aging and Alzheimer disease. medRxiv. 2019 preprint doi:10.1101/2019.12.13.19014902
32. Janelidze S, Bali D, Ashton NJ, et al. Head-to-head comparison of 10 plasma phospho-tau assays in prodromal Alzheimer's disease. *Brain*. 2023;146:1592-1601. doi:10.1093/brain/awac333
33. Lantero-Rodriguez J, Salvadó G, Snellman A, et al. Plasma N-terminal containing tau fragments (NTA-tau): a biomarker of tau deposition in Alzheimer's disease. *Mol Neurodegener*. 2024;19:19. doi:10.1186/s13024-024-00707-x
34. Ashton NJ, Pascoal TA, Karikari TK, et al. Plasma p-tau231: a new biomarker for incipient Alzheimer's disease pathology. *Acta Neuropathol*. 2021;141:709-724. doi:10.1007/s00401-021-02275-6
35. Pereira JB, Janelidze S, Smith R, et al. Plasma GFAP is an early marker of amyloid-$\beta$ but not tau pathology in Alzheimer's disease. *Brain*. 2021;144:3505-3516. doi:10.1093/brain/awab223
36. Thijssen E, La Joie R, Strom AB, et al. Plasma phosphorylated tau 217 and phosphorylated tau 181 as biomarkers in Alzheimer's disease and frontotemporal lobar degeneration: a retrospective diagnostic performance study. *Articles Lancet Neurol*. 2021;20:739-752.
37. Schindler SE, Petersen KK, Saef B, et al. Head-to-head comparison of leading blood tests for Alzheimer's disease pathology. *Alzheimer Dement*. 2024;20:8074-8096. doi:10.1002/alz.14315
38. Pichet Binette A, Franzmeier N, Spotorno N, et al. Amyloid-associated increases in soluble tau relate to tau aggregation rates and cognitive decline in early Alzheimer's disease. *Nat Commun*. 2022;13:6635. doi:10.1038/s41467-022-34129-4
39. Ossenkoppele R, Leuzy A, Cho H, et al. The impact of demographic, clinical, genetic, and imaging variables on tau PET status. *Eur J Nucl Med Mol Imaging*. 2021;48:2245-2258. doi:10.1007/s00259-020-05099-w/Published
40. Ossenkoppele R, Schonhaut DR, Schöll M, et al. Tau PET patterns mirror clinical and neuroanatomical variability in Alzheimer's disease. *Brain*. 2016;139:1551-1567. doi:10.1093/brain/aww027
41. Coomans EM, Tomassen J, Ossenkoppele R, et al. Genetically identical twins show comparable tau PET load and spatial distribution. *Brain*. 2022;145:3571-3581. doi:10.1093/brain/awac004
42. Snoek J, Larochelle H, Adams RP. Practical Bayesian optimization of machine learning algorithms. *Adv Neural Information Process Syst*. 2012;25.
43. Pelikan M, Goldberg DE, Cantú-Paz E. BOA: The Bayesian Optimization Algorithm. Proceedings of the genetic and evolutionary computation conference GECCO-99. 1999;1:525-532.
44. Lundberg SM, Allen PG, Lee S-I. A Unified Approach to Interpreting Model Predictions. 31st Conference on Neural Information Processing Systems, 2017.

15525279, 2025, 2, Downloaded from https://alz-journals.onlinelibrary.wiley.com/doi/10.1002/alz.14400, Wiley Online Library on [11/08/2025]. See the Terms and Conditions (https://onlinelibrary.wiley.com/terms-and-conditions) on Wiley Online Library for rules of use; OA articles are governed by the applicable Creative Commons License

45. Smith R, Hägerström D, Pawlik D, et al. Clinical utility of Tau positron emission tomography in the diagnostic workup of patients with cognitive symptoms. *JAMA Neurol*. 2023;80:749-756. doi:10.1001/jamaneurol.2023.1323
46. Sims JR, Zimmer JA, Evans CD, et al. Donanemab in early symptomatic Alzheimer disease: the TRAILBLAZER-ALZ 2 randomized clinical trial. *JAMA*. 2023;330:512-527. doi:10.1001/jama.2023.13239
47. Hampel H, Au R, Mattke S, et al. Designing the next-generation clinical care pathway for Alzheimer's disease. *Nat Aging*. 2022;2:692-703. doi:10.1038/s43587-022-00269-x
48. Aisen PS, Jimenez-Maggiora GA, Rafii MS, Walter S, Raman R. Early-stage Alzheimer disease: getting trial-ready. *Nat Rev Neurol*. 2022;18:389-399. doi:10.1038/s41582-022-00645-6
49. Lee J, Burkett BJ, Min H-K, et al. Synthesizing images of tau pathology from cross-modal neuroimaging using deep learning. *Brain*. 2024;147:980-995. doi:10.1093/brain/awad346
50. Chen KT, Tesfay R, Koran MEI, et al. Generative adversarial network-enhanced ultra-low-dose [18F]-PI-2620 s PET/MRI in aging and neurodegenerative populations. *Am J Neuroradiol*. 2023;44:1012-1020. doi:10.3174/ajnr.A7961
51. Palmqvist S, Tideman P, Mattsson-Carlgren N, et al. Blood biomarkers to detect Alzheimer disease in primary care and secondary care. *JAMA*. 2024;332:1245-1257. doi:10.1001/jama.2024.13855
52. Jack CR, Wiste HJ, Algeciras-Schimnich A, et al. Predicting amyloid PET and tau PET stages with plasma biomarkers. *Brain*. 2023;146:2029-2044. doi:10.1093/brain/awad042
53. Leuzy A, Smith R, Cullen NC, et al. Biomarker-based prediction of longitudinal Tau positron emission tomography in Alzheimer disease. *JAMA Neurol*. 2022;79:149-158. doi:10.1001/jamaneurol.2021.4654
54. Brum WS, Cullen NC, Therriault J, et al. A blood-based biomarker workflow for optimal tau-PET referral in memory clinic settings. *Nat Commun*. 2024;15. doi:10.1038/s41467-024-46603-2
55. Barthélemy NR, Salvadó G, Schindler S, et al. Highly accurate blood test for Alzheimer's disease comparable or superior to clinical CSF tests. *Nat Med*. 2024;30:1085-1095. doi:10.1038/s41591-024-02869-z
56. Devanarayan V, Charil A, Horie K, et al. Plasma pTau217 ratio predicts continuous regional brain tau accumulation in amyloid-positive early Alzheimer's disease. *Alzheimer Dement*. 2024:1-15. doi:10.1002/alz.14411
57. Vandevrede L, La Joie R, Thijssen EH, et al. Evaluation of plasma phosphorylated Tau217 for differentiation between Alzheimer disease and frontotemporal lobar degeneration subtypes among patients with corticobasal syndrome. *JAMA Neurol*. 2023;80:495-505. doi:10.1001/jamaneurol.2023.0488
58. Mattsson-Carlgren N, Janelidze S, Bateman RJ, et al. Soluble P-tau217 reflects amyloid and tau pathology and mediates the association of amyloid with tau. *EMBO Mol Med*. 2021;13. doi:10.15252/emmm.202114022
59. Horie K, Salvadó G, Barthélemy NR, et al. CSF MTBR-tau243 is a specific biomarker of tau tangle pathology in Alzheimer's disease. *Nat Med*. 2023;29:1954-1963. doi:10.1038/s41591-023-02443-z
60. Joie La R, Visani AV, Baker SL, et al. Prospective longitudinal atrophy in Alzheimer's disease correlates with the intensity and topography of baseline tau-PET. *Sci Transl Med*. 2020;12:5732.
61. Duong MT, Das SR, Lyu X, et al. Dissociation of tau pathology and neuronal hypometabolism within the ATN framework of Alzheimer's disease. *Nat Commun*. 2022;13. doi:10.1038/s41467-022-28941-1
62. Lyu X, Duong MT, Xie L, et al. Tau-neurodegeneration mismatch reveals vulnerability and resilience to comorbidities in Alzheimer's continuum. *Alzheimer Dement*. 2024;20:1586-1600. doi:10.1002/alz.13559
63. Das SR, Lyu X, Duong MT, et al. Tau-Atrophy variability reveals phenotypic heterogeneity in Alzheimer's disease. *Ann Neurol*. 2021;90:751-762. doi:10.1002/ana.26233
64. Vogel JW, Hansson O. Subtypes of Alzheimer's disease: questions, controversy, and meaning. *Trends Neurosci*. 2022;45:342-345. doi:10.1016/j.tins.2022.02.001
65. Harris CR, Millman KJ, van der Walt SJ, et al. Array programming with NumPy. *Nature*. 2020;585:357-362. doi:10.1038/s41586-020-2649-2
66. Mckinney W. Data structures for statistical computing in Python. Proceedings of the 9th Python in Science Conference. 2010:56-61. doi:10.25080/Majora-92bf1922-00a
67. Hunter J. Matplotlib: a 2D graphics environment. *Comput Sci Eng*. 2007;9:90-95. doi:10.1109/MCSE.2007.55
68. Pedregosa F, Michel V, Grisel O, et al. Scikit-learn: Machine Learning in Python. *J Mach Learn Res*. 2011;12:2825-2830.

## SUPPORTING INFORMATION

Additional supporting information can be found online in the Supporting Information section at the end of this article.

**How to cite this article:** Karlsson L, Vogel J, Arvidsson I, et al. Machine learning prediction of tau-PET in Alzheimer's disease using plasma, MRI, and clinical data. *Alzheimer's Dement*. 2025;21:e14600. https://doi.org/10.1002/alz.14600

15525279, 2025, 2, Downloaded from https://alz-journals.onlinelibrary.wiley.com/doi/10.1002/alz.14600, Wiley Online Library on [11/08/2025]. See the Terms and Conditions (https://onlinelibrary.wiley.com/terms-and-conditions) on Wiley Online Library for rules of use; OA articles are governed by the applicable Creative Commons License